

Relativistic BCS-BEC crossover in a boson-fermion model

Jian Deng,^{1,†} Andreas Schmitt,^{2,‡} and Qun Wang^{1,‡}

¹*Department of Modern Physics, University of Science and Technology of China, Anhui 230026, People's Republic of China*

²*Department of Physics, Washington University St Louis, MO 63130, USA*

(Dated: May 5, 2007)

We investigate the crossover from Bardeen-Cooper-Schrieffer (BCS) pairing to a Bose-Einstein condensate (BEC) in a relativistic superfluid within a boson-fermion model. The model includes, besides the fermions, separate bosonic degrees of freedom, accounting for the bosonic nature of the Cooper pairs. The crossover is realized by tuning the difference between the boson mass and boson chemical potential as a free parameter. The model yields populations of condensed and uncondensed bosons as well as gapped and ungapped fermions throughout the crossover region for arbitrary temperatures. Moreover, we observe the appearance of antiparticles for sufficiently large values of the crossover parameter. As an application, we study pairing of fermions with imbalanced populations. The model can potentially be applied to color superconductivity in dense quark matter at strong couplings.

PACS numbers: 12.38.Mh, 11.10.Wx, 03.75.Nt

I. INTRODUCTION

An arbitrarily weak attractive interaction between fermions in a many-fermion system leads to the formation of Cooper pairs. This phenomenon is well described within Bardeen-Cooper-Schrieffer (BCS) theory [1]. In this situation, Cooper pairs are typically of a size much larger than the mean interparticle distance. The picture changes for sufficiently large interaction strengths. In this case, Cooper pairs become bound states, and superfluidity is realized by a Bose-Einstein condensation (BEC) of molecular bosons composed of two fermions. A crossover between the weak-coupling BCS regime and the strong-coupling BEC regime is expected [2].

Experimentally, this crossover has been studied in systems of cold fermionic atoms in a magnetic trap, where the coupling strength can be tuned around a Feshbach resonance with the help of an external magnetic field [3]. Recently, these studies have been extended to the case two fermion species with imbalanced populations [4]. In this case, the crossover is most likely replaced by one or more phase transitions, and the appearance of exotic superfluids seems to be a very interesting possibility [5, 6].

Besides the nonrelativistic atomic systems, there is also a strong motivation to study the relativistic BCS-BEC crossover. One possible realization is pion condensation, which, for large isospin densities, crosses over into Cooper pairing of quarks and antiquarks [7]. Another possibility is dense quark matter which may be present in compact stars [8]. Under astrophysical conditions of densities of a few times the nuclear ground state density and comparably small temperatures of 1 MeV and lower, quark matter is a color superconductor [9, 10]. Analogous to electrons in a metal or alloy or fermionic atoms in a magnetic trap, quarks form Cooper pairs due to an attractive interaction, here mediated by gluon exchange. Because of asymptotic freedom, color superconductivity at asymptotically large densities can be studied in a weak-coupling approach using perturbative methods within QCD [11, 12]. However, for moderate densities as present in compact stars, the validity of these results is questionable. More phenomenological models such as the Nambu-Jona-Lasinio (NJL) model, have therefore been employed, mimicking the gluon exchange by a pointlike interaction between the quarks (see Ref. [13] and references therein). Both QCD and NJL approaches usually are applied within a BCS-like picture. However, quark matter in compact stars may well be in a strong-coupling regime where a BEC-like picture is more appropriate [14–18].

In order to describe the crossover from BCS to BEC we shall not consider a purely fermionic model which may describe this crossover as a function of the fermionic coupling strength. We rather set up a theory with bosonic and fermionic degrees of freedom. Here, fermions and bosons are coupled through a Yukawa interaction and required to be in chemical equilibrium, $2\mu_f = \mu_b$, where μ_f and μ_b are the fermion and boson chemical potentials, respectively. We treat the (renormalized) boson mass m_{br} and the boson-fermion coupling g as free parameters. Then, tuning

Electronic address: djddd@mail.ustc.edu.cn

[†]Electronic address: aschmitt@wuphys.wustl.edu

[‡]Electronic address: qunwang@ustc.edu.cn

the parameter $x = (m_{b;c}^2 / m_b^2) = (4g^2)$ drives the system from the BCS to the BEC regime. The fermionic chemical potential shall be self-consistently determined from the gap equation and charge conservation. This picture is inspired by the boson-fermion model of superconductivity considered in Ref. [19], which has been used in the context of cold fermionic atoms [20]. It also has possible applications for high-temperature superconductivity [21]. For simplicity, we shall restrict ourselves to the evaluation of the model in a mean-field approximation.

The paper is organized as follows. In Sec. II we set up the simplest version of the model, taking into account a single fermion species. We define the crossover parameter in Sec. II C and derive the density and gap equations in Sec. II D. The solutions of these equations are presented in Sec. III. We consider a vanishing temperature in Sec. III A, present the crossover at the critical temperature in Sec. III B, and show results for a fixed crossover parameter and arbitrary temperature in Sec. III C. In Sec. III D we present the results for the ratios ρ_c and T_c . Finally, we extend our model to two fermion species in Sec. IV. This extension allows us to consider pairing of fermions with imbalanced populations, which is an unavoidable complication in quark matter at moderate densities [22].

Our convention for the metric tensor is $g = \text{diag}(1; -1; -1; -1)$. Our units are $\hbar = c = k_B = 1$. Four-vectors are denoted by capital letters, $K = (k_0; \mathbf{k})$ with $k = |\mathbf{k}|$. Fermionic Matsubara frequencies are $i\omega_n = i(2n + 1) \pi T$, while bosonic ones are $i\omega_n = i2n \pi T$ with the temperature T and n an integer.

II. THE BOSON-FERMION MODEL FOR A RELATIVISTIC SUPERFLUID

A. Setting up the model

We use a model of fermions and composite bosons coupled to each other by a Yukawa interaction. The Lagrangian is given by a free fermion part L_f , a free boson part L_b and an interaction part L_I ,

$$L = L_f + L_b + L_I; \quad (1)$$

with

$$L_f = \int d^4x \bar{\psi} (i \not{\partial} + m) \psi; \quad (2a)$$

$$L_b = \int d^4x [\partial_\mu \phi^\dagger \partial^\mu \phi - m_b^2 \phi^\dagger \phi]; \quad (2b)$$

$$L_I = \int d^4x g (\bar{\psi} \psi \phi + \text{h.c.}); \quad (2c)$$

The fermions are described by the spinor ψ , while the bosons are given by the complex scalar field ϕ . The charge conjugate spinors are defined by $\bar{\psi} = \psi^\dagger \gamma^0$ and $\bar{\phi} = \phi^\dagger$ with $C = i \gamma^2 \gamma^0$. The fermion (boson) mass is denoted by m (m_b). We choose the boson chemical potential to be twice the fermion chemical potential,

$$\mu_b = 2\mu_f; \quad (3)$$

Therefore, the system is in chemical equilibrium with respect to the conversion of two fermions into one boson and vice versa. This allows us to model the transition from weakly-coupled Cooper pairs made of two fermions into a molecular difermionic bound state, described as a boson. The interaction term accounts for a local interaction between fermions and bosons with coupling constant g . In order to describe BEC of the bosons, we have to separate the zero mode of the field ϕ [23]. Moreover, we shall replace this zero-mode by its expectation value

$$\phi_0 = \langle \phi \rangle; \quad (4)$$

and neglect the interaction between the fermions and the *non-zero* boson modes. This corresponds to the mean-field approximation. Then, with the Nambu-Gorkov spinors

$$\Psi = \begin{pmatrix} \psi \\ \bar{\psi} \end{pmatrix}; \quad \bar{\Psi} = (\bar{\psi} \quad \psi); \quad (5)$$

the Lagrangian can be written as

$$L = \frac{1}{2} \bar{\Psi} S^{-1} \Psi + \int d^4x [\partial_\mu \phi^\dagger \partial^\mu \phi - m_b^2 \phi^\dagger \phi] + \int d^4x g (\bar{\Psi} \Psi \phi + \text{h.c.}); \quad (6)$$

Note that we have dropped the mixing terms of zero and non-zero boson modes since they vanish when carrying out the path integral. Here S^{-1} is the inverse fermion propagator which reads in momentum space

$$S^{-1}(p) = \begin{pmatrix} p \cdot \gamma + m & 0 \\ 0 & -p \cdot \gamma + m \end{pmatrix} + \frac{2ig}{2\pi} \begin{pmatrix} 0 & 1 \\ 1 & 0 \end{pmatrix}; \quad (7)$$

It is instructive to compare this form of the propagator to the corresponding one in a purely fermionic model, see for instance Ref. [15]. As expected, the Bose condensate is related to the diquark condensate ,

$$= 2g : \quad (8)$$

As we shall see below, cf. Eq. (11), is the energy gap in the quasi-fermion excitation spectrum. In a purely fermionic model, $= 2G\hbar^{-1}$, where G is the coupling constant related to the interaction between the fermions. Note that G has mass dimension -2 , while our boson-fermion coupling g is dimensionless. Therefore, g does not play the role of the crossover parameter, as G does in the fermionic model. We shall explain this in more detail in Sec. II C.

B. Thermodynamic potential

In order to obtain the thermodynamical potential density , we compute the partition function

$$Z = \int \mathcal{D}[\bar{\psi}, \psi, \bar{\phi}, \phi] \exp \left(- \int_0^{\beta} d\tau \int d^3x L \right) ; \quad (9)$$

where T is the temperature, and L is the Lagrangian in the mean field approximation given in Eq. (6). The thermodynamic potential density is then obtained from $= -T/V \ln Z$, where V is the volume of the system. One obtains after performing the path integral and the sum over Matsubara frequencies,

$$= \sum_{e=\pm 1} \int \frac{d^3k}{(2\pi)^3} \left(\epsilon_k^e + 2T \ln \left(1 + \exp \left(-\frac{\epsilon_k^e}{T} \right) \right) \right) + \frac{(m_b^2 - \epsilon_b^2)}{4g^2} + \frac{1}{2} \sum_{e=\pm 1} \int \frac{d^3k}{(2\pi)^3} \left(\epsilon_k^e + 2T \ln \left(1 + \exp \left(-\frac{\epsilon_k^e}{T} \right) \right) \right) : \quad (10)$$

We have used Eq. (8) and denoted the quasi-particle energy for fermions ($e = +1$) and antifermions ($e = -1$) by

$$\epsilon_k^e = \sqrt{(k_0 - e\epsilon)^2 + \epsilon^2}; \quad \epsilon_{k0} = \sqrt{k^2 + m^2}; \quad (11)$$

and the (anti)boson energy by

$$\epsilon_k^e = \sqrt{k^2 + m_b^2} - e\epsilon_b : \quad (12)$$

Furthermore, we have assumed (and thus) to be real.

C. Crossover parameter

We shall now define the crossover parameter whose variation carries the system from the BCS to the BEC regime. Let us first recall the corresponding crossover parameter in a purely fermionic model. In this case, the fermionic coupling G has to be renormalized. This is in contrast to the weak-coupling regime where the gap equation is well-defined with the bare coupling G (a natural cutoff is provided by the Debye frequency in the non-relativistic case; in QCD, the gap is a function of momentum and peaks around the Fermi surface, providing a regular behavior of the gap equation). The renormalized coupling is proportional to the scattering length. In the context of cold fermionic atoms, the scattering length is the physical quantity which can be controlled upon tuning the external magnetic field. For the relativistic case, see Ref. [17] for the relation between the renormalized coupling and the scattering length. The definition of the crossover parameter in the present model goes along the same lines. Instead of a renormalized coupling we introduce the renormalized boson mass

$$m_{br}^2 = 4g^2 \frac{\epsilon}{\epsilon^2} \Big|_{\epsilon = T=0} = m_b^2 - 4g^2 \int \frac{d^3k}{(2\pi)^3} \frac{1}{\epsilon_{k0}} : \quad (13)$$

This allows us to define the (renormalized) crossover parameter

$$\propto \frac{m_{br}^2 - m_b^2}{4g^2} : \quad (14)$$

The parameter x can be varied from negative values with large modulus (BCS) to large positive values (BEC). In between, $x = 0$ is the unitary limit [24–26]. Therefore, $1/x$ behaves similar to the scattering length: the BCS (BEC) limit is approached via $1/x \rightarrow 0$ ($1/x \rightarrow \infty$) while the unitary regime corresponds to $1/x = -1$.

We may thus write the thermodynamical potential in terms of the parameters $(x; g)$ instead of the original pair $(m_b; g)$. To this end, we have to express the bare boson mass m_b in terms of x and g . With the help of Eqs. (13) and (14) we find

$$m_b^2 = 4g^2 \int_0^\Lambda \frac{d^3k}{(2\pi)^3} \frac{1}{k^2 + x} = 4g^2 (x_0 - x) : \quad (15)$$

For sufficiently small fermion masses, $m \rightarrow 0$, where Λ is the cutoff in the momentum integrals, we have

$$x_0 = \frac{\Lambda^2}{4} : \quad (16)$$

One sees from Eq. (15) that x_0 is an upper limit for x in order to ensure non-negative bosonic occupation numbers. Moreover, in the limit of large $x \rightarrow x_0$ the boson chemical potential approaches the (bare) boson mass, $\mu_b \rightarrow m_b$. The condition of Bose-Einstein condensation in a free bosonic system with fixed bosonic charge is $\mu_b = m_b$. In the present model, however, we shall observe a nonzero Bose condensate also for $\mu_b < m_b$, corresponding to $x < x_0$.

Having defined the crossover parameter x and its definition range $x \in [-1; x_0]$, we note that, within our simple model, we are left with the second free parameter g . We shall discuss below how the choice of g effects the behavior of the system in the BCS-BEC crossover. For most of our results we shall, however, use a single fixed value of g .

D. Densities and gap equation

Next, we derive the charge conservation equation and the gap equation which shall later be solved numerically. The total charge density

$$n = \frac{\partial \Omega}{\partial \mu} \quad (17)$$

can, using Eq. (10), be written as

$$n = n_F + n_0 + n_B : \quad (18)$$

Here, the fermionic contribution is given by

$$n_F = 2 \sum_{\mathbf{k}} \int_0^\Lambda \frac{d^3k}{(2\pi)^3} \frac{1}{2\epsilon_{\mathbf{k}}} [f_F(\epsilon_{\mathbf{k}}) - f_F(\epsilon_{\mathbf{k}}^e)] ; \quad (19)$$

where we abbreviated

$$\epsilon_{\mathbf{k}}^e = \epsilon_{\mathbf{k}} - \mu = \epsilon_{\mathbf{k}} - \mu_b ; \quad (20)$$

and f_F is the Fermi distribution function, $f_F(x) = 1/[\exp(x/T) + 1]$. The factor 2 in front of the sum in Eq. (19) originates from the two spin degrees of freedom. From Eq. (19) one recovers the limit case of a free Fermi gas at zero temperature,

$$n_F(\mu = T = 0) = \frac{(\frac{1}{2} m^2)^{3/2}}{6\pi^2} [1 - (\frac{m}{\mu})^2] : \quad (21)$$

The condensate density is

$$n_0 = \frac{m_b^3}{6\pi^2} ; \quad (22)$$

and the thermal boson contribution is

$$n_B = 2 \sum_{\mathbf{k}} \int_0^\Lambda \frac{d^3k}{(2\pi)^3} f_B(\epsilon_{\mathbf{k}}^e) ; \quad (23)$$

where f_B is the Bose distribution function, $f_B(x) = 1/[\exp(x/T) + 1]$. The factor 2 in the boson densities originates from Eq. (3), i.e., from the fact that each boson is composed of two fermions. For the following, let us also define the charge fractions

$$n_B = \frac{n_{B=F}}{n}; \quad n_0 = \frac{n_0}{n}; \quad (24)$$

and an effective Fermi momentum p_F through

$$n = \frac{p_F^3}{3\pi^2}; \quad (25)$$

The effective Fermi energy is then given by $\epsilon_F = \frac{p_F^2}{2m}$. The various densities appearing on the right-hand side of Eq. (18) are interpreted as follows. The fermions that contribute to n_F are, for temperatures below the superfluid transition temperature, constituents of weakly coupled Cooper pairs. For temperatures larger than the transition temperature, n_F corresponds to free fermions. The bosons that contribute to the boson density n_B are, for all temperatures, *uncondensed* molecular bound states, composed of two fermions. Condensation of these pairs can only occur below the transition temperature and results in a nonzero condensate density n_0 .

In order to find the gap equation in the case of a fixed charge density, we have to minimize the free energy density

$$F = \epsilon + \mu n; \quad (26)$$

Here, ϵ is an implicit function of n (and of the gap Δ) through Eq. (17). Minimization with respect to Δ yields

$$0 = \frac{dF}{d\Delta} = \frac{\partial \epsilon}{\partial \Delta} + \frac{\partial \epsilon}{\partial \Delta} \frac{\partial \Delta}{\partial \mu} + n \frac{\partial \mu}{\partial \Delta} = \frac{\partial \epsilon}{\partial \Delta}; \quad (27)$$

where Eq. (17) has been used. For $\mu \neq 0$ Eq. (27) reads

$$x = \frac{\sum_{\mathbf{k}} \int_0^{\Delta} \frac{d^3 k}{(2\pi)^3} \frac{1}{2\epsilon_{\mathbf{k}}} \tanh \frac{\epsilon_{\mathbf{k}}}{2T} - \frac{1}{2k_0}}{\mu}; \quad (28)$$

Note that the density n in Eq. (18) was obtained by taking the derivative with respect to μ at fixed m_b (not at fixed x). This is necessary to obtain a nonzero condensate contribution n_0 . Also the equivalence of $dF/d\Delta = 0$ and $\partial \epsilon / \partial \Delta = 0$ in Eq. (27) is obtained under this premise. At fixed m_b we get μ by solving Eqs. (18) and (28). We can then obtain x from m_b and μ via Eq. (14). In this way we have a one-to-one mapping between m_b and x . Here we should emphasize that the current case is different from that x is fixed from the very beginning before Eq. (18) is derived.

III. RESULTS AND DISCUSSION

The two coupled equations (18) and (28) with the definitions (19), (22), and (23) shall be used in the following to determine the gap Δ , and the chemical potential μ as functions of the crossover parameter x , see Eq. (14), and the temperature T at fixed effective Fermi momentum p_F , fermion mass m , and boson-fermion coupling g . The solution $[\Delta(x; T), \mu(x; T)]$ can then, in turn, be used to compute the densities of fermions and bosons in the x - T plane. We shall present results for the zero-temperature case, Sec. III A, and at the critical temperature T_c , Sec. III B. Then, we show results for a fixed x and arbitrary temperature T , Sec. III C. Throughout these subsections, we shall fix

$$\frac{p_F}{m} = 0.3; \quad \frac{m}{g} = 0.2; \quad g = 4; \quad (29)$$

In Sec. III D we present the ratios $\Delta_0 = \Delta_0$ and $T_{c0} = T_{c0}$ for different values of m and g as a function of x . Here and in the following, we use the subscript 0 at Δ_0 and T_{c0} to denote the zero-temperature value.

A. Zero temperature

For $T = 0$, there are no thermal bosons, $n_B = 0$, and Eqs. (18) and (28) become

$$n = n_F + n_0; \quad (30a)$$

$$x = \frac{\sum_{\mathbf{k}} \int_0^{\Delta} \frac{d^3 k}{(2\pi)^3} \frac{1}{2\epsilon_{\mathbf{k}}} - \frac{1}{2k_0}}{\mu}; \quad (30b)$$

with the zero-temperature expressions for the fermion densities

$$n_F = \frac{1}{2} \int_{e=0}^{\infty} \frac{d^3k}{(2\pi)^3} \frac{e^{-\epsilon_k}}{2\epsilon_k} : \quad (31)$$

The numerical results for the solution of the coupled equations (30a) and (30b) are shown in Fig. 1. The left panel shows the fermion chemical potential μ_0 and the gap Δ_0 as functions of x . In the weak-coupling regime (small x) we see that the chemical potential is given by the Fermi energy, $\mu_0 = \epsilon_F$. For the given parameters, $\epsilon_F = 0.36$. The chemical potential decreases with increasing x and approaches zero in the far BEC region. The gap is exponentially small in the weak-coupling region, as expected from BCS theory. It becomes of the order of the chemical potential around the unitary limit, $x = 0$, and further increases monotonically for positive x . In the unitary limit, we have $\mu_0 = 0.37$, while in nonrelativistic fermionic models $\mu_0 = 0.4$ – 0.5 was obtained [24–26].

The corresponding fermion and boson densities are shown in the right panel of Fig. 1. These two curves show the crossover: at small x all Cooper pairs are resonant states, which is characterized by a purely fermionic density, $n = n_F$; at large x , on the other hand, Cooper pairs are bound states and hence there are no fermions in the system. The charge density is rather dominated by a bosonic condensate, $n = n_0$. The crossover region is located around $x = 0$. We can characterize this region quantitatively as follows. We write the boson mass as $m_B = 2m - E_{\text{bind}}$. Then, a bound state appears for positive values of the binding energy E_{bind} , i.e., for $2m > m_B$. With Eq. (15) this inequality reads

$$\frac{1}{2} < m^2 - g^2(x_0 - x) : \quad (32)$$

Since μ_0 is a monotonically decreasing function of x , this relation suggests (note that $x_0 - x > 0$ by construction): (i) for sufficiently large $x < x_0$ bound states appear for any fixed g (ii) the larger g the “later” (= larger values of x) bosonic states appear. We have confirmed these two statements numerically by using different values of g . The value $g = 4$ is chosen such that there is an approximately balanced coexistence of fermions and bosons at $x = 0$, $n_F \approx n_0$, as can be seen in the right panel of Fig. 1.

One may ask whether there is a contribution of antifermions to the total fermion charge. In the BCS regime there is a Fermi surface given by $\epsilon > 0$ and antifermion excitations are obviously suppressed. However, during the crossover, μ_0 decreases and there might be the possibility of the appearance of antifermions. The contributions of fermions and antifermions to the total fermion charge seem to be given by the terms $e = +1$ and $e = -1$ in Eq. (31). A separate discussion of these terms is not straightforward because they contain divergent contributions which cancel in the sum but not in each term separately. Thus, a renormalization of both terms would be required. In the BCS regime, $x \ll 1$, vacuum contributions $\propto \Lambda^3$ have to be subtracted. For nonzero values of the gap, however, more divergent terms appear, involving powers of both the cutoff and the gap. (Note that this problem is not unlike the one encountered in Ref. [27], where medium-dependent counter terms were introduced in the calculation of the Meissner mass. In fact, we shall choose a similar renormalization in the following calculation of the energy density.)

In any case, separate charges of fermions and antifermions are not measurable quantities since any potential experiment would solely measure the total charge. Therefore, we shall describe the onset of a nonzero antiparticle population in terms of the energy density. In this quantity, we expect the contributions from particles and antiparticles to add up, in contrast to the charge density where the contributions (partially) cancel each other.

Let us first discuss the quasi-fermion and quasi-antifermion excitation energies given by ϵ_k^+ and ϵ_k^- from Eq. (11). Inserting the numerical solutions for μ_0 and Δ_0 into these energies results in the curves shown in Fig. 2. These excitation energies show that, for large values of x , quasi-fermions and quasi-antifermions become degenerate due to the vanishingly small chemical potential. Because of the large energy gap, we expect neither quasi-fermions nor quasi-antifermions to be present in the system.

This statement can be made more precise and generalized to nonzero temperatures upon considering the energy density E . Using the thermodynamic potential density Ω from Eq. (10) and the entropy density $S = -\partial\Omega/\partial T$ we have $E = \Omega + nT$. We obtain

$$E = E_F + E_B ; \quad (33)$$

with the fermionic and bosonic contributions

$$E_F = \int_{e=0}^{\infty} \frac{d^3k}{(2\pi)^3} \epsilon_k^e [1 - 2f_F(\epsilon_k^e)] + n_F ; \quad (34a)$$

$$E_B = \frac{1}{2} \int_{e=0}^{\infty} \frac{d^3k}{(2\pi)^3} \epsilon_k^e [1 + 2f_B(\epsilon_k^e)] + (x_0 - x)^2 + (n_0 + n_B) : \quad (34b)$$

The renormalization of the fermionic part can now be chosen such that there are no quasi-particles at $T = n_F = 0$, in accordance with the above argument. Hence we subtract the “vacuum contribution” $E_F(T = n_F = 0)$ to obtain the renormalized energy density

$$E_{F,r} = 2 \int_e^Z \frac{d^3k}{(2\pi)^3} \epsilon_k f_F(\epsilon_k) + n_F : \quad (35)$$

For $T = 0$, only the second term survives (remember that $\epsilon_k > 0$), and E_F behaves as shown in the left panel of Fig. 3. For nonzero temperatures, however, we see that there is a nonzero fermionic energy density even for $n_F = 0$. This is related to the excitation of quasi-antifermions, as we shall discuss in the next subsection.

For the bosonic energy density, we subtract the analogous vacuum part $E_B(T = n_0 + n_B = 0)$. Hence we obtain the renormalized energy density

$$E_{B,r} = 2 \int_e^Z \frac{d^3k}{(2\pi)^3} \epsilon_k f_B(\epsilon_k) + (n_0 + n_B) : \quad (36)$$

At $T = 0$, we have $E_{B,r} = n_0$, which is shown in the left panel of Fig. 3. We see that the bosonic energy density vanishes in the BCS regime because there is no Bose condensate in this case, $n_0 = 0$. In the far BEC regime, where $n_0 \neq 0$, the energy density vanishes too because the boson chemical potential, since coupled to the fermion chemical potential, vanishes. Only in the crossover region, where both the condensate and the chemical potential are nonzero, the energy density is nonvanishing.

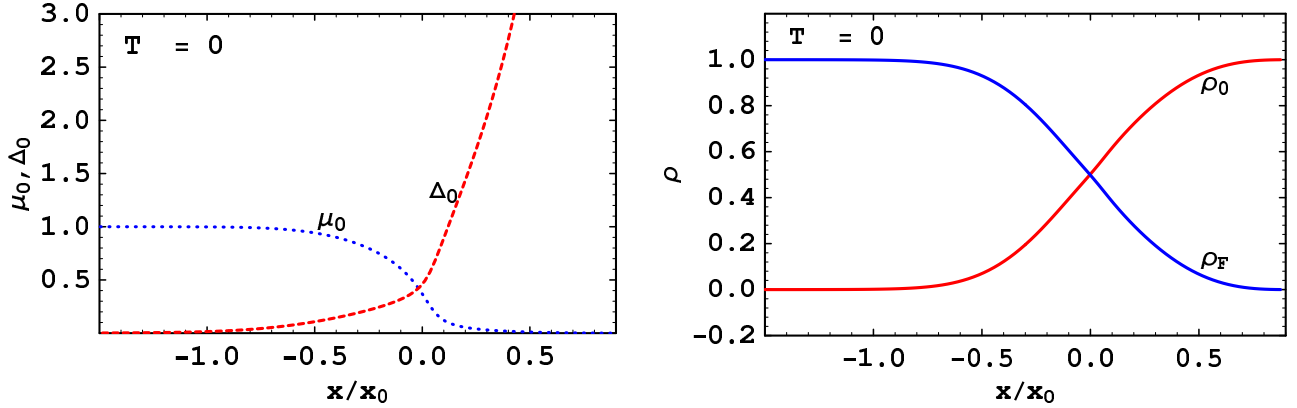


Figure 1: (Color online) Crossover at zero temperature from the BCS regime (small x) to the BEC regime (large x). Left panel: fermion chemical potential μ_0 (blue dotted) and gap Δ_0 (red dashed) in units of effective Fermi energy ϵ_F . Right panel: condensate fraction (red solid), fermion fraction (blue solid).

B. Critical temperature

In this section, we calculate the critical temperature T_c and the corresponding particle densities as functions of x . Upon setting $\mu = 0$ in the charge density equation (18) and the gap equation (28) one obtains

$$n = n_F + n_B ; \quad (37a)$$

$$x = 2 \int_e^Z \frac{d^3k}{(2\pi)^3} \frac{1}{2\epsilon_k} \tanh \frac{\epsilon_k}{2T_c} - \frac{1}{2k_0} ; \quad (37b)$$

with the fermion density

$$n_F = 2 \int_e^Z \frac{d^3k}{(2\pi)^3} f_F(\epsilon_k) ; \quad (38)$$

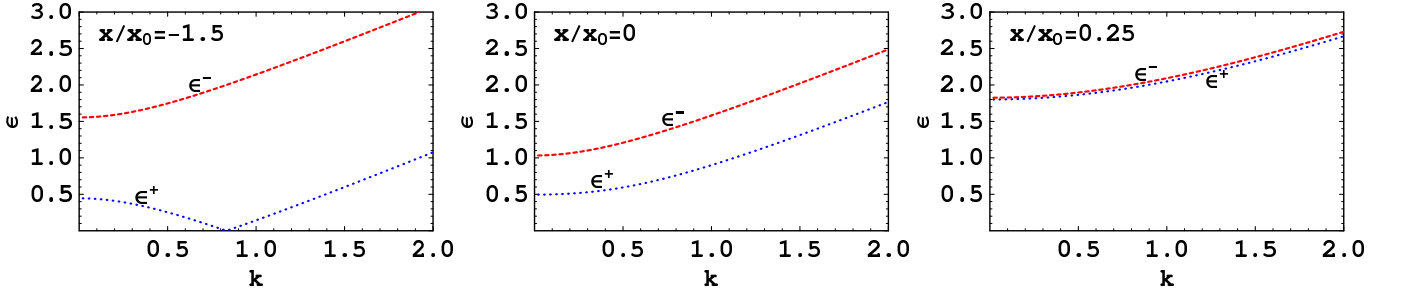


Figure 2: (Color online) Fermion and antifermion excitation energies ϵ_k^+ and ϵ_k^- as defined in Eq. (11) for three different values of the crossover parameter x/x_0 at $T = 0$ as a function of the momentum k (both ϵ_k and k are given in units of ϵ_F). In the BCS regime (left panel) the energy gap is small and the fermion excitations are well separated from antifermion excitations. Both excitations approach each other in the unitary regime (middle panel), and become indistinguishable in the far BEC regime (right panel). Note in particular that the minimum of the antiparticle excitation is not a monotonic function of x .

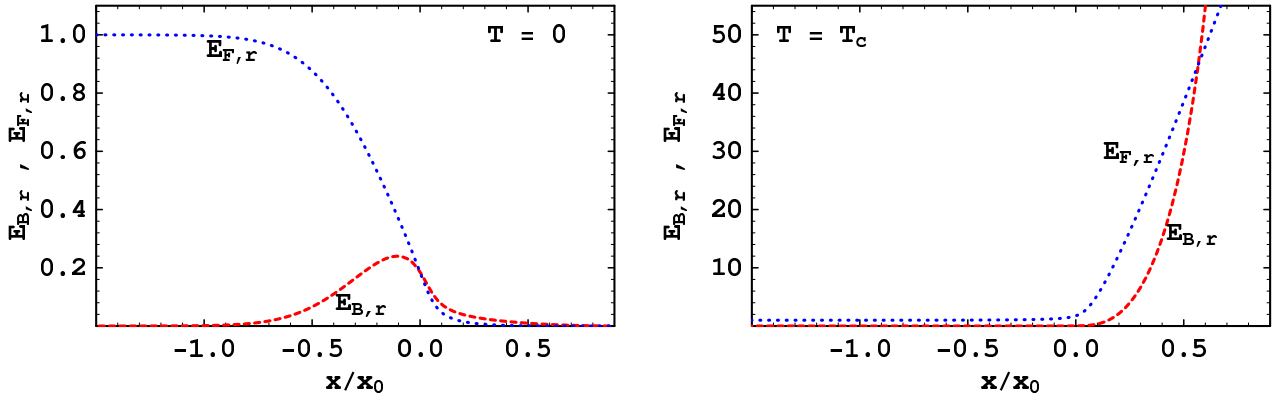


Figure 3: (Color online) Energy density of fermions and bosons in units of $\epsilon_F n$ at $T = 0$ (left panel) and at $T = T_c$ (right panel). In the BCS regime, $E_F = \epsilon_F n$ and $E_B = 0$ for all temperatures. The large fermionic and bosonic energy densities in the BEC regime at $T = T_c$ indicate the occupation of (quasi-)antiparticle modes.

and the boson density given by Eq. (23). Strictly speaking, the original gap equation (28) is only valid for nonzero μ (in its derivation, one has to divide by μ). Therefore, Eq. (37b) has to be understood as a limit for approaching the critical temperature from below, $T \nearrow T_c$, i.e., for infinitesimally small μ . Eqs. (37a) and (37b) can now be used to determine T_c and the corresponding chemical potential μ_c .

The results are shown in the left panel of Fig. 4. We see that the chemical potential behaves qualitatively as for zero temperature. The critical temperature, while exponentially small in the BCS regime, becomes of the order of and then larger than the chemical potential during the crossover. This is one of the characteristics of the strong coupling regime and one reason why this model (in its nonrelativistic version) is used to describe high-temperature superconductivity [21]. In Sec. IIID we use the ratio T_c/μ_c to illustrate the high- T_c behavior.

The right panel of Fig. 4 shows the particle density fractions for fermions and bosons. A crossover similar to the zero-temperature case can be seen. The density fractions of fermions and bosons suggest that the crossover is shifted to a slightly larger value of x compared to the zero-temperature case. While at zero temperature $n_F = n_0$ occurs at $x=x_0 \nearrow 0$, here we have $n_F = n_B$ at $x=x_0 \nearrow 0.3$. It is clear that there is no Bose condensate at $T = T_c$; the bosonic population rather consists of thermal molecules. These are uncondensed, strongly-coupled Cooper pairs (see Ref. [28] for a recent discussion of this effect in the context of cold atoms). We see that uncondensed pairs do not exist in the BCS limit. In this case, the superfluid phase transition occurs “abruptly”, with pair formation and condensation at the same temperature.

In the right panel of Fig. 3 we show the fermion and boson energy densities. These curves are obtained by inserting the solutions for μ_c and T_c into Eq. (35) and (36) and making use of $\mu = 0$. We see that, in contrast to the zero-temperature case, the fermionic energy density increases with x despite $n_F \nearrow 0$. This is easy to understand from the

corresponding quasi-fermion excitations. For all temperatures, the vanishing chemical potential renders quasi-particles and quasi-antiparticles degenerate. Whereas at $T = 0$ they are both gapped by Δ , at $T = T_c$ they are gapped only by the fermion mass m . For large values of x we have $T_c \rightarrow m$ and quasi-fermions as well as quasi-antifermions can be thermally excited. In this context, it would be interesting to consider the formation of chiral condensates which may be initiated by the degeneracy of quasi-fermions and quasi-antifermions. We leave this extension of the model for future studies.

The large increase of the bosonic energy density can be understood in the same way. Note, however, that, in contrast to the fermion mass, the boson mass decreases with increasing crossover parameter x . This difference, together with the different statistics of bosons and fermions gives rise to the qualitatively different behavior of E_B/x compared to E_F/x . The strong increase of antiparticle densities has also been predicted in other models and has been termed “relativistic BEC (RBEc)” [16, 17]. The relativistic effects have also been studied in Ref. [18].

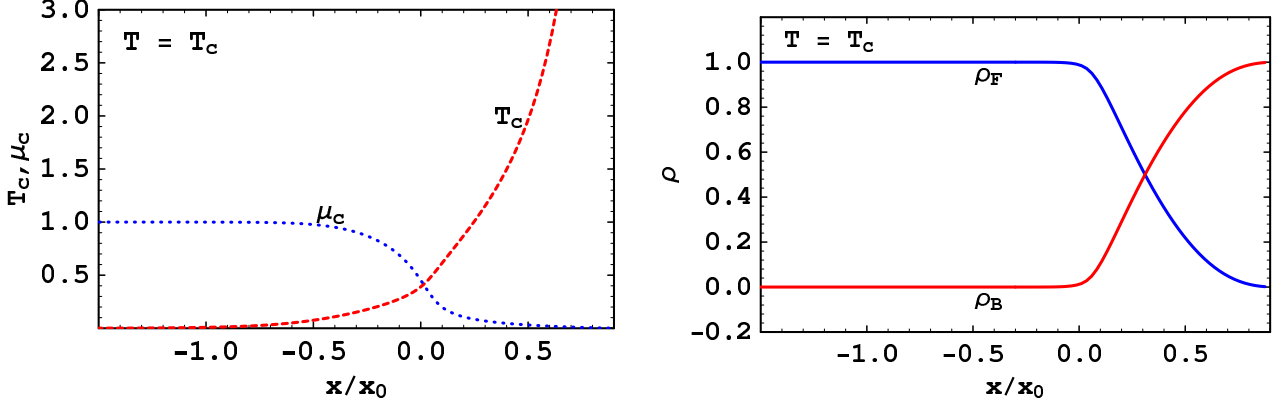


Figure 4: (Color online) Crossover at the critical temperature. Left panel: fermion chemical potential μ_c (blue dotted) and critical temperature T_c (red dashed) in units of the effective Fermi energy E_F . Right panel: fermion fraction (blue solid), thermal boson fraction (red solid).

C. Fixed coupling

In the previous two subsections we have presented the solution of Eqs. (18) and (28) along two lines in the x - T plane: along the line $T = 0$ (Sec. III A) and along the (curved) line $T = T_c$ (Sec. III B). Now we explore a third path by fixing the crossover parameter and vary the temperature from zero to values beyond T_c . We shall use $x = x_0 = 0.2$ which is in the intermediate-coupling regime, where both fermionic and bosonic populations are present. For $T < T_c$, we use Eqs. (18) and (28) to determine μ and Δ . For $T > T_c$, the gap vanishes, $\Delta = 0$, i.e., we have the single equation (37a) to determine the chemical potential μ .

The condensate and the fermion and boson density fractions are shown in Fig. 5. At the left end, $T = 0$, one recovers the results shown in Fig. 1 at the particular value $x = x_0 = 0.2$, while the point $T = T_c = 1$ reproduces the respective result shown in Fig. 4. The second-order phase transition manifests itself in a kink in the density fractions and a vanishing condensate. Below T_c we observe coexistence of condensed bound states, condensed resonant states, and, for sufficiently large temperatures, uncondensed bound states. We obtain thermal bosons even above the phase transition. They can be interpreted as “preformed” pairs, just as the uncondensed pairs below T_c . This phenomenon is also called “pseudogap” in the literature [28, 29]. It suggests that there is a temperature $T^*(x)$ which marks the onset of pair formation. This temperature is not necessarily identical to T_c . In the BCS regime, $T^*(x) = T_c(x)$, while for $x \ll 0$, $T^*(x) > T_c(x)$. Of course, our model does not predict any quantitative value for T^* because thermal bosons are present for all temperatures. Therefore, we expect the model to be valid only for a limited temperature range above T_c .

D. The ratios $\rho_0 = \rho_0$ and $T_c = \rho_0$

We finally present the results for the ratios $\rho_0 = \rho_0$, and $T_c = \rho_0$. They shall serve as a discussion of the dependence of our results on the boson-fermion coupling g and the fermion mass m . Both g and m were fixed throughout the

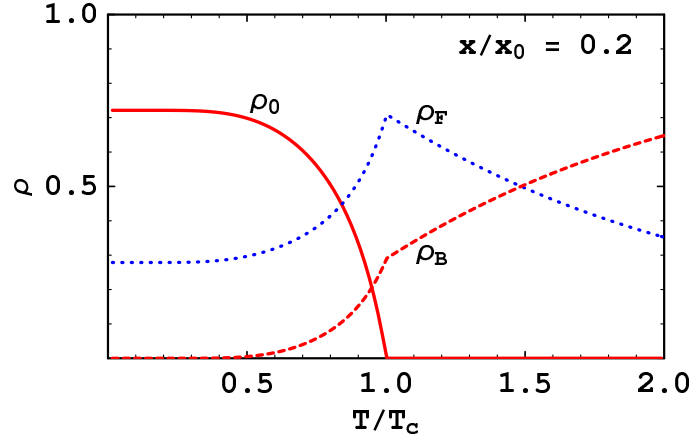


Figure 5: (Color online) Density fractions in the crossover regime at fixed $x/x_0 = 0.2$ as functions of temperature: condensed bosons (red solid), fermions and uncondensed bosons (blue dotted and red dashed, respectively).

previous sections. Moreover, we shall see that we reproduce values of these ratios obtained in different models in certain limit cases.

Fig. 6 shows the ratio $\rho_0 = \rho_0$, using the results for ρ_0 and ρ_0 from Sec. III A. From both panels one can read off the value of the ratio in the unitary limit, $x \rightarrow 0$. For the fermion mass that has been used in the previous subsections, $m = m_0 = 0.2$, we find $1.2 \leq \rho_0 = \rho_0 \leq 1.4$. The exact value depends on the choice of g . This range is in agreement with nonrelativistic, purely fermionic models [24–26]. The right panel shows that the ratio in the unitary limit decreases with decreasing fermion mass. In particular, in the ultrarelativistic limit $m = 0$ we find $\rho_0 = \rho_0 \approx 1.0$.

In Fig. 7 we show the ratio $T_c = T_c$, using the result for T_c from Sec. III B. From BCS theory we know

$$\lim_{x \rightarrow 1} \frac{T_c}{T_c} = \frac{e}{\gamma} \approx 0.57; \quad (39)$$

where $\gamma \approx 0.577$ is the Euler-Mascheroni constant. This value is reproduced in our results, independent of g and m . Upon increasing the crossover parameter x , the ratio deviates from its BCS value and increases substantially during the crossover where it strongly depends on the coupling g . Therefore we make no predictions for its value in the unitary regime. However, we see that in the BEC regime, the value again becomes independent of the parameters and assumes a value

$$\lim_{x \rightarrow x_0} \frac{T_c}{T_c} \approx 0.50; \quad (40)$$

IV. TWO-SPECIES SYSTEM WITH IMBALANCED POPULATIONS

It is straightforward to extend our boson-fermion model to two fermion species with cross-species pairing. This allows us to introduce a mismatch in fermion numbers and chemical potentials which imposes a stress on the pairing. This kind of stressed pairing takes place in a variety of real systems. For example, quark matter in a compact star is unlikely to exhibit standard BCS pairing in the color-flavor locked (CFL) phase, i.e., pairing of quarks at a common Fermi surface. The cross-flavor (and cross-color) pairing pattern of the CFL phase rather suffers a mismatch in chemical potentials in the pairing sectors bu and bd (rs and bs meaning red, green, blue, and u; d; s meaning up, down, strange). This mismatch is induced by the explicit flavor symmetry breaking through the heaviness of the strange quark and by the conditions of color and electric neutrality. Our system shall only be an idealized and simplified model of this complicated scenario. However, as in the previous sections, we shall allow for arbitrary values of the crossover parameter and thus model the strong coupling regime of quark matter. We shall fix the overall charge and the difference in the two charges. This is comparable to the effect of neutrality conditions for matter inside a compact star, which also impose constraints on the various color and flavor densities. Our focus will be to find stable homogeneous superfluids in the crossover region and, by discarding the unstable solutions, identify parameter values where the crossover in fact becomes a phase transition. We shall restrict ourselves to zero temperature and defer the full analysis of the two-species system to a future study [30].

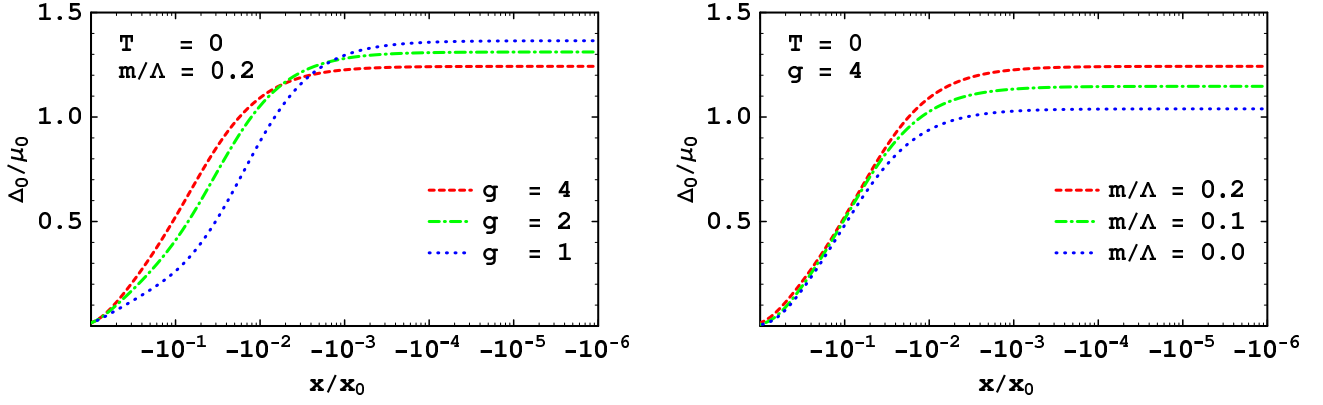


Figure 6: (Color online) Ratio of gap over chemical potential at zero temperature for crossover parameters $x=x_0 < 0$ on a logarithmic scale. The left end of the horizontal axis corresponds to the BCS regime, the right end, where $x \rightarrow 0$, corresponds to the unitary regime. Left panel: ratio for different values of the boson-fermion coupling g . Right panel: ratio for different values of the fermion mass.

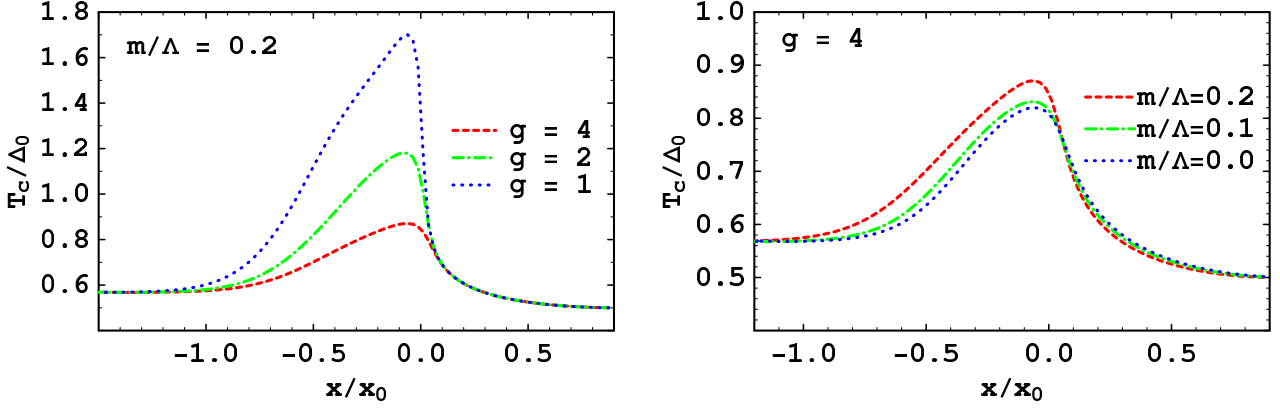


Figure 7: (Color online) Ratio of critical temperature over zero-temperature gap throughout the BCS-BEC crossover. Left panel: ratio for different values of the boson-fermion coupling g . Right panel: ratio for different values of the fermion mass.

A. Two-fermion system

We start by replacing the fermion spinor in the Lagrangian (1) with a two-component spinor

$$\psi = \frac{1}{\sqrt{2}} \begin{pmatrix} \psi_1 \\ \psi_2 \end{pmatrix}; \quad (41)$$

and the chemical potential with the matrix $\text{diag}(\mu_1; \mu_2)$. The factor $1/\sqrt{2}$ accounts for the same normalization for the total fermion number as in the case of single fermion species. We assume both fermions to have the same mass m . Cross-species pairing is taken into account in the interaction part of the Lagrangian L_I in (2c) which is now replaced by

$$L_I = g(\psi^\dagger_{c1} \psi_{s1} + \psi^\dagger_{s1} \psi_{c1}); \quad (42)$$

where the Pauli matrix σ_1 is a matrix in the two-species space. We denote the average chemical potential and the mismatch in chemical potentials by

$$\mu = \frac{\mu_1 + \mu_2}{2}; \quad \delta\mu = \frac{\mu_1 - \mu_2}{2}; \quad (43)$$

Then, the bosonic chemical potential is

$$\mu_b = 2\bar{\mu} : \quad (44)$$

The thermodynamic potential differs from the one-fermion case in the dispersion relation for the fermions,

$$\begin{aligned} \Omega = & \frac{m_b^2}{4g^2} \frac{1}{2} + \frac{1}{2} \sum_e \int \frac{d^3k}{(2\pi)^3} \left[\epsilon_k^e + 2T \ln(1 - e^{-\epsilon_k^e/T}) \right] \\ & + \sum_e \int \frac{d^3k}{(2\pi)^3} \left[\epsilon_k^e + T \ln(1 + e^{-(\epsilon_k^e + \bar{\mu})/T}) \right] + T \ln(1 + e^{-(\epsilon_k^e - \bar{\mu})/T}) ; \end{aligned} \quad (45)$$

where

$$\epsilon_k^e = \sqrt{(k_0 - \bar{\mu})^2 + m^2} \quad (46)$$

and ϵ_k^e as in Eq. (12). At zero temperature it becomes

$$\Omega = \frac{m_b^2}{4g^2} \frac{1}{2} + \sum_e \int \frac{d^3k}{(2\pi)^3} [\epsilon_k^e + (\epsilon_k^e - \bar{\mu}) \theta(\epsilon_k^e - \bar{\mu})] : \quad (47)$$

The particle number densities for each species are derived from the thermodynamic potential,

$$n_i = -\frac{\partial \Omega}{\partial \mu_i} = \frac{n_0}{2} + n_{f,i}; \quad (i = 1, 2); \quad (48)$$

where n_0 is given by Eq. (22) and

$$n_{f,i=2} = \sum_e \int \frac{d^3k}{(2\pi)^3} \frac{e^{-\epsilon_k^e/T}}{2\epsilon_k^e} e^{-(\epsilon_k^e - \bar{\mu})/T} : \quad (49)$$

We shall evaluate the model for fixed sum and difference of the particle number densities

$$\bar{n} = n_1 + n_2 = -\frac{\partial \Omega}{\partial \bar{\mu}} = n_0 + \sum_e \int \frac{d^3k}{(2\pi)^3} \frac{e^{-\epsilon_k^e/T}}{\epsilon_k^e} (\epsilon_k^e - \bar{\mu}); \quad (50a)$$

$$n = n_1 - n_2 = -\frac{\partial \Omega}{\partial \mu} = \sum_e \int \frac{d^3k}{(2\pi)^3} (\epsilon_k^e - \bar{\mu}); \quad (50b)$$

Of course, the bosons contribute equally to both particle numbers and thus do not appear in n . The gap equation becomes

$$x = \sum_e \int \frac{d^3k}{(2\pi)^3} (\epsilon_k^e - \bar{\mu}) \frac{1}{2\epsilon_k^e} - \frac{1}{2k_0} : \quad (51)$$

We shall solve Eqs. (50) and (51) for the variables $\bar{\mu}$, μ , and x .

B. Possible Fermi surface topologies

Before we solve the equations, let us comment on their structure, in particular the appearance of the step function. It is convenient to rewrite the step functions such that their effect can be translated into the boundaries of the $d\mathbf{k}$ integration. Furthermore, it is instructive to discuss the different particle and antiparticle occupation numbers in momentum space with the help of the step functions. As we shall see, the occupation numbers are discontinuous at the zeros of the dispersion relation ϵ_k^e . We assume without loss of generality that $\bar{\mu} > 0$ (in the numerical solution we ensure this by choosing $\bar{\mu} > 0$). We abbreviate

$$- \frac{1}{2} \frac{1}{\epsilon_k^e} = \frac{1}{2} \frac{1}{\epsilon_k^e} ; \quad \epsilon_k^e = m^2 : \quad (52)$$

cases	characteristics	parameter region	$N_{f,i}^+(\mathbf{k})$ (fermions)	$N_{f,i}(\mathbf{k})$ (anti-fermions)
I	fully gapped	$< \text{ or } + < m$	$N_{f1}^+ = N_{f2}^+ = N_{\text{gap}}^+$	$N_{f1} = N_{f2} = N_{\text{gap}}$
II	breached for fermions gapped for anti-fermions	$m < < +$	$N_{f1}^+ = 1, N_{f2}^+ = 0, k \in [0; \frac{P}{+}]$ $N_{f1}^+ = N_{f2}^+ = N_{\text{gap}}^+, k \notin [0; \frac{P}{+}]$	same as case I
III	single EFS for fermions gapped for anti-fermions	$j < j < m < +$	$N_{f1}^+ = 1, N_{f2}^+ = 0, k \in [0; \frac{P}{+}]$ $N_{f1}^+ = N_{f2}^+ = N_{\text{gap}}^+, k \notin [0; \frac{P}{+}]$	same as case I
IV	single EFS for fermions single EFS for anti-fermions	$m < < +$	same as case III	$N_{f1} = 0, N_{f2} = 1, k \in [0; \frac{P}{+}]$ $N_{f1} = N_{f2} = N_{\text{gap}}, k \notin [0; \frac{P}{+}]$

Table I: Four possible parameter configurations and corresponding fermion ($e = +$) and antifermion ($e = -$) occupation numbers $N_{f,i}^e(\mathbf{k})$ ($i = 1, 2$). The occupation numbers are defined as the integrand in Eq. (49). We abbreviate “effective Fermi surface” by EFS and $N_{\text{gap}}^e = e(\frac{e}{k} - \frac{e}{k}) = (2 \frac{e}{k})$. The different cases are illustrated in Fig. 8.

Then, the step functions are

$$\left(\frac{+}{k} \right) = \left(\frac{+}{k} \right) \left(\frac{+}{k} \right) \left(\frac{P}{+} - k \right) \left(\frac{+}{k} \right) \left(\frac{+}{k} \right) \left(\frac{P}{+} - k \right); \quad (53a)$$

$$\left(\frac{-}{k} \right) = \left(\frac{-}{k} \right) \left(\frac{-}{k} \right) \left(\frac{-}{k} \right) \left(\frac{P}{-} - k \right); \quad (53b)$$

We see that the step functions only give a contribution if $k > 0$. Three different terms occur, each corresponding to a different scenario, distinguished by the topology of the effective Fermi surfaces of fermions and antifermions. Together with the fully gapped state, these are four possible cases. We list these cases and their characteristics in Table I and Fig. 8. The fermion dispersion ($e = +$) has either zero, one, or two zeros. A zero corresponds to an effective Fermi sphere. In particular, a fully gapped state is characterized by the disappearance of any Fermi surface. The case of two effective Fermi surfaces is termed “breached pairing”, following the usual terminology [31]. The antifermion dispersion ($e = -$), in contrast, can have either zero or one effective Fermi surfaces. Here, the asymmetry between fermions and antifermions is given by the choice $\frac{P}{-} > 0$. Hence there is no breached pairing for antifermions. We find the interesting possibility of filled Fermi surfaces for fermions of species 1 and antifermions of species 2, see case IV in Table I and lower right panel in Fig. 8. In Sec. IV D we shall see that this is indeed a stable solution for certain values of the crossover parameter.

C. Number susceptibilities

In order to check the gapless states for their stability, we have to compute the number susceptibility matrix [5, 6]

$$\chi_{ij} = \frac{dn_i}{d\mu_j}; \quad i = 1, 2; \quad (54)$$

Note that we fix \bar{n} and n (or equivalently n_1 and n_2) in our solution. Hence χ can be regarded as measuring the response of the system to a small perturbation away from this solution. In particular, a stable solution requires the mismatch in density to increase for an increasing mismatch in chemical potentials. Therefore, a negative eigenvalue of this 2×2 matrix indicates the instability of a given solution. The susceptibility is evaluated upon using

$$\chi_{ij} = \frac{1}{2} \frac{dn_0}{d\mu_j} + \frac{dn_{f,i}}{d\mu_j} = \frac{2}{2g^2} + \frac{2}{g^2} + \frac{\partial n_{f,i}}{\partial \mu_j} \frac{\partial}{\partial \mu_j} + \frac{\partial n_{f,i}}{\partial \mu_j}; \quad (55)$$

The partial derivatives of the fermion densities with respect to the gap and chemical potentials are straightforwardly computed with the help of Eq. (49). The partial derivative of the gap with respect to the chemical potentials can be computed from the gap equation. To this end, we take the (total) derivative with respect to $\mu_{1=2}$ on both sides of Eq. (51) and solve the equation for $\partial \mu = \partial \mu_{1=2}$. The results for the various terms are given in Appendix A.

D. Stable and unstable gapless superfluids

We first present the results for a certain mismatch in densities,

$$\frac{n}{\bar{n}} = 0.5; \quad (56)$$

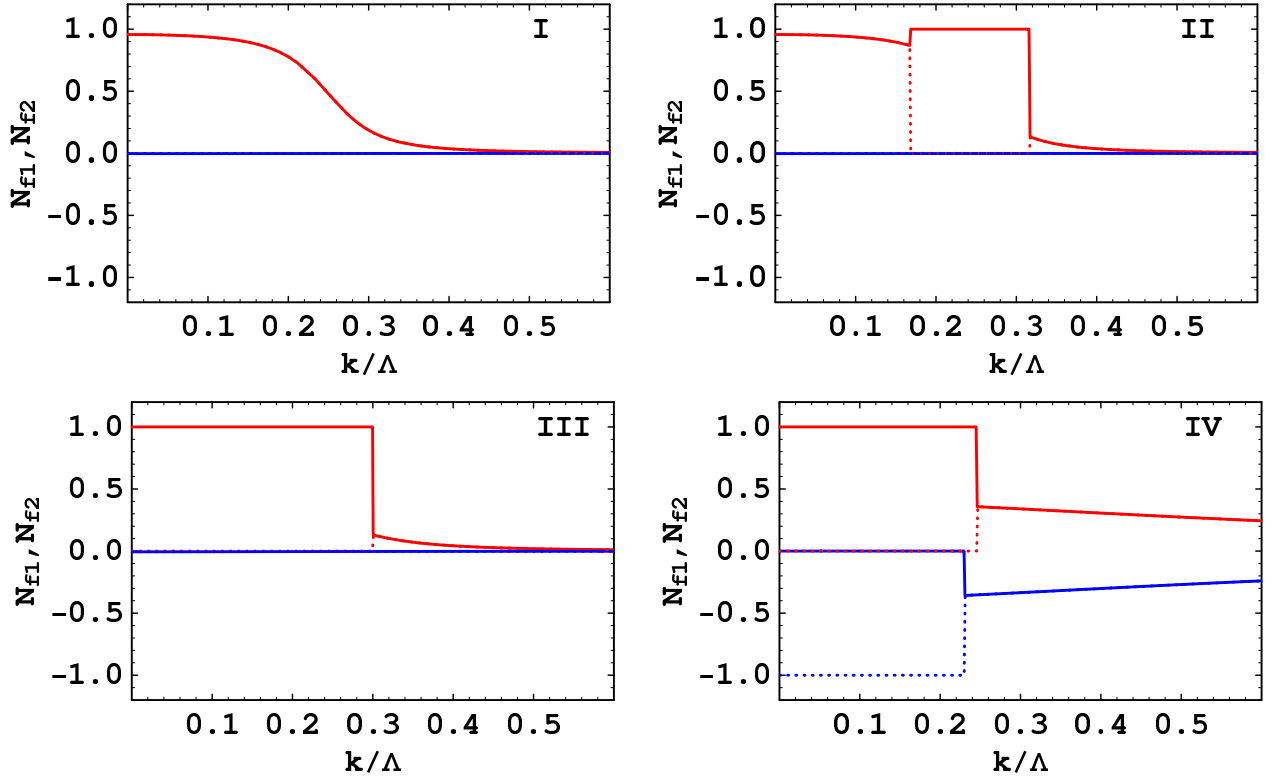


Figure 8: (Color online) Occupation numbers for fermions (red) and anti-fermions (blue). Solid and dotted lines are for species 1 and 2 respectively. The panels illustrate the qualitatively different cases I through IV from Table I. Note that dotted and solid lines coincide in various regions, e.g., for all k in the upper left panel. See last two columns of Table I for the precise form of the occupation numbers.

Moreover, we use $\bar{n} = p_F^3/(3\pi^2)$, and p_F, m, g , as in the main part of the paper, see Eq. (29). Then, for $T = 0$ we have a set of coupled equations (50) and (51) for any value of the crossover parameter x . We solve this set of equations for μ, Δ , and α . The results are shown in Fig. 9. The left panel shows that the behavior of the average chemical potential and the gap are not unlike the case with a single fermion species, cf. Fig. 1. Moreover, we see that $\mu > 0$ for all x . This is clear from Eq. (50b): any nonzero Δ goes along with $\mu > 0$. In other words, the standard fully gapped pairing does not allow (at $T = 0$) for a difference in fermion numbers. Thus all solutions correspond to gapless pairing and case I in Table I and Fig. 8 does not appear. We have indicated in Fig. 9 for which values of x which of the cases II, III, and IV occurs. We have also marked the onset of instability. Evaluation of the susceptibility matrix $\chi_{ij}(\mathbf{k})$ yields negative eigenvalues for $x \in [0.04x_0, x_+]$ and $x \in [0.28x_0, x_+]$. In fact, one of the eigenvalue diverges at these points. Denoting the two eigenvalues of χ by λ_1, λ_2 , we have

$$\lambda_1 = \begin{cases} +1 & \text{for } x \neq x_-; x \neq x_+ \\ -1 & \text{for } x = x_-; x = x_+ \end{cases}; \quad (57a)$$

$$\lambda_2 > 0 \text{ for all } x; \quad (57b)$$

Unstable regions of negative λ_1 are shaded in both panels of the figure. We see that the breached pair solution is always unstable. This is expected from similar results from mean-field studies for nonrelativistic systems [6] as well as quark matter (gapless CFL and 2SC phases [32]). Interestingly, the stable region consists of two qualitatively distinct states, labelled by III and IV. The system accounts for a given difference in number densities not only by filling an effective Fermi surface with particles of species 1 (state III), but also by additionally filling an anti-Fermi surface of species 2 (state IV). An interesting feature of this state is that in the limit of equal Fermi surfaces (1 and anti-2) all charges (n_1 and n_2) are confined in the Fermi sphere, just as in the unpaired phase. This can be seen from the lower right panel in Fig. 8: the total occupation numbers for momenta larger than the effective Fermi momentum vanish since particle and antiparticle contributions cancel each other. Before this limit is reached, however, this state becomes unstable for $x > x_+$. This instability in the BEC regime is in contrast to nonrelativistic systems, where a gapless solution (there with a single effective Fermi surface) persists throughout the BEC region [5].

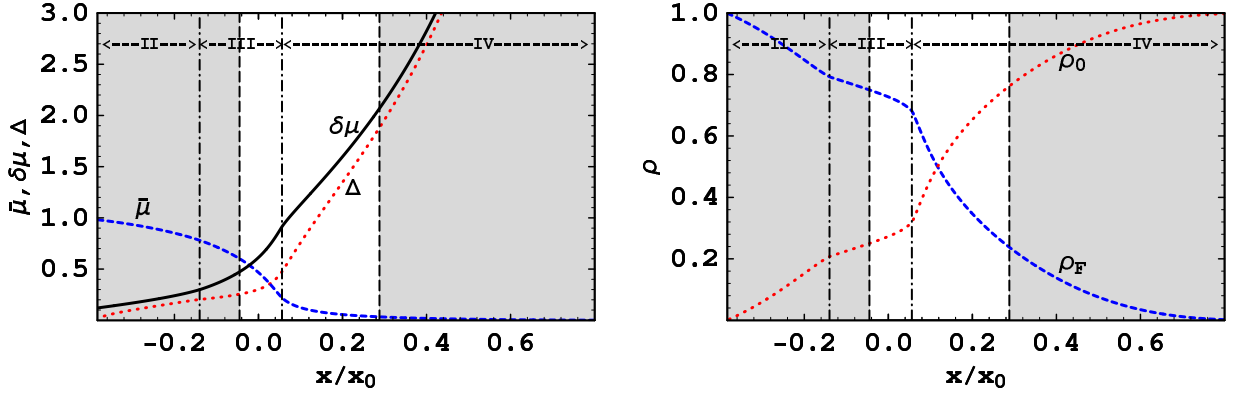


Figure 9: (Color online) The crossover with imbalanced population at zero temperature. Left panel: μ (blue dashed), Δ (black solid) and $\delta\mu$ (red dotted) in units of ϵ_F for fixed \bar{n} and \bar{n} . Right panel: bosonic (red dotted) and fermionic (blue dashed) density fractions. The shaded parameter regions are unstable with respect to a negative susceptibility. The states II, III, and IV correspond to the respective Fermi surface topologies discussed in Table I.

The right panel of Fig. 9 shows the bosonic and fermionic number density fractions, cf. Fig. 1 for the analogous curves without mismatch. Taking the value of x where $\rho_0 = \rho_F$ as an indicator, we see that the BCS-BEC crossover is shifted to a larger value of x ($x' > 0$ vs. $x' = 0 \pm x_0$). Of course, what was a crossover in Fig. 1 is now actually replaced by at least two phase transitions. The regions marked as unstable will be replaced by a different phase. It is beyond the scope of this paper to determine these phases, but it can be expected that they are spatially inhomogeneous, for instance a mixed phase where a superfluid and normal phases are spatially separated, or some kind of “Larkin-Ovchinnikov-Fulde-Ferrell” (LOFF) state [33]. In the stable region we see that the change in Fermi surface topologies (from state III to IV) is visible in the boson and fermion fractions which exhibit a kink at this point.

We finally present a phase diagram in Fig. 10 for arbitrary (positive) values of $\bar{n} = \bar{n}$. Since we do not consider spatially inhomogeneous phases, this phase diagram is incomplete. Its main point is to identify regions where homogeneous gapless superfluids may exist. We find that for sufficiently large mismatches, $\bar{n} = \bar{n} \approx 0.02$ there is a region where no solution with nonzero Δ can be found (we have not shown this region in the above results for $\bar{n} = \bar{n} = 0.5$). We see that the region of stable superfluids shrinks with increasing $\bar{n} = \bar{n}$, as expected. Note that the horizontal axis $\bar{n} = \bar{n} = 0$ is not continuously connected to the rest of the phase diagram. For vanishing mismatch in densities a stable, fully gapped superfluid exists for all x , as we saw in the main part of the paper. One should thus not be misled by the instability for arbitrarily small mismatches.

We conclude with emphasizing the two main qualitative differences to analogous phase diagrams in nonrelativistic systems: (i) within the stable region of homogeneous gapless superfluids there is a curve that separates two different Fermi surface topologies; this is the right dashed-dotted line in Fig. 10. (ii) for large x the gapless superfluid becomes unstable even in the far BEC region; this is the shaded area on the right side in Fig. 10.

V. SUMMARY AND OUTLOOK

We have studied the relativistic BCS-BEC crossover for zero and nonzero temperatures within a boson-fermion model. Variations of this model have previously been used for nonrelativistic systems in order to study cold fermionic atoms and high-temperature superconductors. The bosons of the model are bound states of fermion pairs. Conversion of two fermions into a boson and vice versa is implemented by requiring chemical equilibrium with respect to this process. The crossover is realized by varying an effective coupling strength x , constructed from the difference between the renormalized boson mass m_{br} and the boson chemical potential μ_b , and the boson-fermion coupling constant g , $x = (m_{br}^2 - \mu_b^2)/(4g^2)$. In this form, $1/x$ plays the role of the scattering length, in particular $1/x = -1$ in the unitary limit. We have evaluated the model in its simplest form, employing a mean-field approximation.

An important property of the model is the coexistence of weakly-coupled Cooper pairs with condensed and uncondensed bosonic bound states. In the crossover regime as well as in the BEC regime, strongly-bound molecular Cooper pairs exist below and above the critical temperature T_c . Above T_c , they are all uncondensed (“preformed” Cooper pairs) while below T_c a certain fraction of them forms a Bose-Einstein condensate. In contrast, in the BCS regime, pairing and condensation of fermionic degrees of freedom (in the absence of bosons) both set in at T_c .

Furthermore, we have characterized the onset of nonzero antifermion and antiboson populations during the crossover by computing the energy density. The reason for the appearance of antiparticles is the strong decrease of the fermion

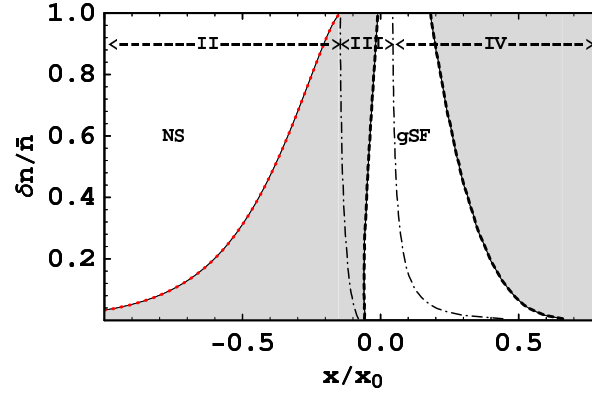


Figure 10: The phase diagram in the plane of the crossover parameter x and the density difference $\delta n/\bar{n}$. Shaded areas have unstable homogeneous solutions with negative number susceptibility. NS denotes “normal state”; in this region, no solution for the gap equation is found. gSF denotes “gapless superfluid”; in this region a stable gapless superfluid state is found with two different Fermi surface topologies, divided by the right dashed-dotted line. The labels II, III, and IV refer to the states listed in Table I.

chemical potential. While the fermion chemical potential is identical to the Fermi energy in the BCS regime, it reaches values well below the fermion mass in the BEC regime. As a consequence, particle and antiparticle excitation energies become almost identical and thus antiparticles are present for nonvanishing temperatures.

Finally, we have extended the model by considering two fermion species with mismatched densities. This case has been evaluated for zero temperature. We have found stable gapless superfluids in the crossover region. In contrast to nonrelativistic systems, we found no stable homogeneous phase in the far BEC region. Moreover, two different stable Fermi surface configurations have been identified. Besides a state with a single effective Fermi surface, also found in nonrelativistic systems, we found the possibility of a superfluid phase with Fermi surfaces for particles of species 1 and anti-particles of species 2. A complete evaluation of the two-species model, including inhomogeneous phases and nonzero temperatures, remains to be done in the future.

The model may be extended in several ways, in order to describe more realistic scenarios, for instance dense quark matter in the interior of a compact star. First, one may go beyond the mean field approximation, which seems particularly interesting in the crossover region, where the validity of this approximation is questionable. Also, one may introduce more than two fermion species, accounting for color and flavor degrees of freedom in quark matter. Finally, we propose to include chiral condensates into the model.

Acknowledgments

A.S. acknowledges valuable discussions with M. Alford, S. Reddy, I. Shovkovy, and support by the U.S. Department of Energy under contracts DE-FG02-91ER50628 and DE-FG01-04ER0225 (OJI). Q.W. thanks P.-f. Zhuang for helpful discussions and is supported in part by the startup grant from University of Science and Technology of China (USTC) in association with ‘Bai Ren’ project of Chinese Academy of Sciences (CAS) and by National Natural Science Foundation of China (NSFC) under the grant 10675109.

Appendix A: CALCULATION OF NUMBER SUSCEPTIBILITIES

In this appendix, we compute the elements of the number susceptibility matrix as given in Eq. (55). For a compact notation we introduce the following abbreviations for integrals containing a δ -function

$$1 \quad \chi_{ee}^X = \int \frac{d^3k}{(2\pi)^3} \frac{e_k^e}{2} \frac{e_k^e}{2} \delta(\epsilon_k^e - \epsilon_k^e); \quad (A1a)$$

$$2 \quad \chi_{ee}^X = \int \frac{d^3k}{(2\pi)^3} \frac{e_k^e}{2} \frac{e_k^e}{2} \delta(\epsilon_k^e - \epsilon_k^e); \quad (A1b)$$

$$3 \quad \chi_{ee}^X = \int \frac{d^3k}{(2\pi)^3} \frac{1}{4} \frac{1}{(\epsilon_k^e)^2} \delta(\epsilon_k^e - \epsilon_k^e); \quad (A1c)$$

and integrals containing a step function

$$\chi_1^Z = \int \frac{d^3k}{(2\pi)^3} \frac{e^{-\epsilon_k}}{2(\epsilon_k)^3} \left(\epsilon_k \right); \quad (A2a)$$

$$\chi_2^Z = \int \frac{d^3k}{(2\pi)^3} \frac{1}{4(\epsilon_k)^3} \left(\epsilon_k \right); \quad (A2b)$$

In this notation the various terms in Eq. (55) become

$$\frac{\partial n_{f;1=2}}{\partial \mu} = \chi_1 - \chi_2; \quad (A3)$$

and

$$\frac{\partial n_{f;1=2}}{\partial \mu_{1=2}} = \chi_2 + \chi_3; \quad \frac{\partial n_{f;1=2}}{\partial \mu_{2=1}} = \chi_2 - \chi_3; \quad (A4)$$

The partial derivative of the gap with respect to the chemical potentials, obtained from the gap equation, is

$$\frac{\partial \Delta}{\partial \mu_{1=2}} = \frac{2(-g^2 + \chi_1 - \chi_3)}{4(\chi_2 - \chi_3)}; \quad (A5)$$

Consequently,

$$\chi_{11=22} = \frac{\chi_2^2}{2g^2} + \chi_2 + \chi_3 + \frac{(2(-g^2 + \chi_1 - \chi_3))^2}{4(\chi_2 - \chi_3)} \quad (A6a)$$

$$\chi_{12} = \chi_{21} = \frac{\chi_2^2}{2g^2} + \chi_2 - \chi_3 + \frac{(2(-g^2 + \chi_1 - \chi_3))(2(-g^2 + \chi_1 + \chi_3))}{4(\chi_2 - \chi_3)} \quad (A6b)$$

In particular, we see that the susceptibility matrix is symmetric.

We may further evaluate the terms with the ϵ -functions. For any function $f^e(k)$ we have

$$\chi_e^Z = \int \frac{d^3k}{(2\pi)^3} f^e(k) \left(\epsilon_k \right) = \frac{(\chi_2 - \chi_3)}{2\pi^2} \left[\left(\frac{p}{2} \right) \left(\frac{p}{2} \right) + f^+ \left(\frac{p}{2} \right) \right. \\ \left. + \left(\frac{p}{2} \right) \left(\frac{p}{2} \right) - \left[\left(\frac{p}{2} \right) f^+ \left(\frac{p}{2} \right) + \left(\frac{p}{2} \right) f \left(\frac{p}{2} \right) \right] \right]; \quad (A7)$$

with χ_2 and χ_3 defined in Eq. (52). Consequently,

$$\chi_1 = \frac{1}{2\pi^2} \frac{(\chi_2 - \chi_3)}{2} \left[\left(\frac{p}{2} \right) \left(\frac{p}{2} \right) + h + \left(\frac{p}{2} \right) \left(\frac{p}{2} \right) - h \operatorname{sgn} \left(\frac{p}{2} \right) \right]; \quad (A8a)$$

$$\chi_2 = \frac{1}{2\pi^2} \frac{(\chi_2 - \chi_3)}{4} \left[\left(\frac{p}{2} \right) \left(\frac{p}{2} \right) + h^2 + \left(\frac{p}{2} \right) \left(\frac{p}{2} \right) - h^2 \operatorname{sgn} \left(\frac{p}{2} \right) \right]; \quad (A8b)$$

$$\chi_3 = \frac{1}{2\pi^2} \frac{(\chi_2 - \chi_3)}{4} \left[\left(\frac{p}{2} \right) \left(\frac{p}{2} \right) + + \left(\frac{p}{2} \right) \left(\frac{p}{2} \right) - \operatorname{sgn} \left(\frac{p}{2} \right) \right]; \quad (A8c)$$

where we abbreviated

$$h = \frac{p}{2} \frac{p}{2}; \quad (A9)$$

For the integrals with the step function we make use of Eqs. (53) to find for any function $f^e(k)$

$$\chi_e^Z = \int \frac{d^3k}{(2\pi)^3} f^e(k) \left(\epsilon_k \right) = \chi_e^Z = \int \frac{d^3k}{(2\pi)^3} f^e(k) \frac{(\chi_2 - \chi_3)}{2\pi^2} \left[\left(\frac{p}{2} \right) \left(\frac{p}{2} \right) + \int_0^{\frac{p}{2}} dk k^2 f^+ \left(\frac{p}{2} \right) \right. \\ \left. + \left(\frac{p}{2} \right) \left(\frac{p}{2} \right) - \int_0^{\frac{p}{2}} dk k^2 f^+ \left(\frac{p}{2} \right) + \left(\frac{p}{2} \right) \left(\frac{p}{2} \right) - \int_0^{\frac{p}{2}} dk k^2 f \left(\frac{p}{2} \right) \right]; \quad (A10)$$

We insert Eqs. (A8) and Eq. (A10) (the latter with the respective integrand replacing $f^e(\mathbf{k})$) into Eq. (A6) to evaluate the susceptibility matrix

-
- [1] J. Bardeen, L.N. Cooper, and J.R. Schrieffer, Phys. Rev. **108**, 1175 (1957).
 - [2] D. M. Eagles, Phys. Rev. **186**, 456 (1969); A. J. Leggett, in *Modern Trends in the Theory of Condensed Matter*, Springer-Verlag (1980); P. Nozieres and S. Schmitt-Rink, J. Low. Temp. Phys. **59**, 195 (1985).
 - [3] C.A. Regal, M. Greiner, and D.S. Jin, Phys. Rev. Lett. **92**, 040403 (2004) [arXiv:cond-mat/0401554]; M. Bartenstein *et. al.*, Phys. Rev. Lett. **92**, 120401 (2004) [arXiv:cond-mat/0401109]; M.W. Zwierlein *et. al.*, Phys. Rev. Lett. **92**, 120403 (2004) [arXiv:cond-mat/0403049]; J. Kinast *et. al.*, Phys. Rev. Lett. **92**, 150402 (2004) [arXiv:cond-mat/0403540]; T. Bourdel *et. al.*, Phys. Rev. Lett. **93**, 050401 (2004) [arXiv:cond-mat/0403091].
 - [4] M. W. Zwierlein, A. Schirotzek, C. H. Schunck and W. Ketterle, Science **311**, 492 (2006) [arXiv:cond-mat/0511197]; G. B. Partridge, W. Li, R. I. Kamar, Y. Liao and R. G. Hulet, Science **311**, 503 (2006) [arXiv:cond-mat/0511752].
 - [5] C.-H. Pao, S.-T. Wu, S.-K. Yip, Phys. Rev. B **73**, 132506 (2006); *ibid*, **74**, 189901 (E) (2006) [arXiv:cond-mat/0506437]; D. T. Son and M. A. Stephanov, Phys. Rev. A **74**, 013614 (2006) [arXiv:cond-mat/0507586]; M. Mannarelli, G. Nardulli and M. Ruggieri, Phys. Rev. A **74**, 033606 (2006) [arXiv:cond-mat/0604579]; Q. Chen, Y. He, C.-C. Chien, K. Levin, Phys. Rev. A **74**, 063603 (2006) [arXiv:cond-mat/0608454]; D. E. Sheehy and L. Radzihovsky, Phys. Rev. B **75**, 136501 (2007).
 - [6] E. Gubankova, A. Schmitt and F. Wilczek, Phys. Rev. B **74**, 064505 (2006) [arXiv:cond-mat/0603603].
 - [7] D. T. Son and M. A. Stephanov, Phys. Rev. Lett. **86**, 592 (2001) [arXiv:hep-ph/0005225]; D. T. Son and M. A. Stephanov, Phys. Atom. Nucl. **64**, 834 (2001) [Yad. Fiz. **64**, 899 (2001)] [arXiv:hep-ph/0011365]; L. y. He, M. Jin and P. f. Zhuang, Phys. Rev. D **71**, 116001 (2005) [arXiv:hep-ph/0503272]; G. f. Sun, L. He and P. Zhuang, arXiv:hep-ph/0703159.
 - [8] J. C. Collins and M. J. Perry, Phys. Rev. Lett. **34**, 1353 (1975).
 - [9] B. C. Barrois, Nucl. Phys. B **129**, 390 (1977); D. Bailin and A. Love, Phys. Rept. **107**, 325 (1984).
 - [10] For reviews, see K. Rajagopal and F. Wilczek, arXiv:hep-ph/0011333; S. Reddy, Acta Phys. Polon. B **33**, 4101 (2002) [arXiv:nucl-th/0211045]; D. H. Rischke, Prog. Part. Nucl. Phys. **52**, 197 (2004) [arXiv:nucl-th/0305030]; M. Alford, Prog. Theor. Phys. Suppl. **153**, 1 (2004) [arXiv:nucl-th/0312007]; H. c. Ren, arXiv:hep-ph/0404074; M. Huang, Int. J. Mod. Phys. E **14**, 675 (2005) [arXiv:hep-ph/0409167]; I. A. Shovkovy, Found. Phys. **35**, 1309 (2005) [arXiv:nucl-th/0410091]; T. Schäfer, arXiv:hep-ph/0509068.
 - [11] D. T. Son, Phys. Rev. D **59**, 094019 (1999) [arXiv:hep-ph/9812287]; D. K. Hong, V. A. Miransky, I. A. Shovkovy and L. C. R. Wijewardhana, Phys. Rev. D **61**, 056001 (2000) [Erratum-ibid. D **62**, 059903 (2000)] [arXiv:hep-ph/9906478]; W. E. Brown, J. T. Liu and H. c. Ren, Phys. Rev. D **61**, 114012 (2000) [arXiv:hep-ph/9908248]; R. D. Pisarski and D. H. Rischke, Phys. Rev. D **61**, 074017 (2000) [arXiv:nucl-th/9910056].
 - [12] For recent developments in color superconductivity using perturbative QCD, see Q. Wang and D. H. Rischke, Phys. Rev. D **65**, 054005 (2002) [arXiv:nucl-th/0110016]; A. Schmitt, Q. Wang and D. H. Rischke, Phys. Rev. D **66**, 114010 (2002) [arXiv:nucl-th/0209050]; A. Ipp, A. Gerhold and A. Rebhan, Phys. Rev. D **69**, 011901 (2004) [arXiv:hep-ph/0309019]; Q. Wang, J. Phys. G **30**, S1251 (2004) [arXiv:nucl-th/0404017]; P. T. Reuter, Q. Wang and D. H. Rischke, Phys. Rev. D **70**, 114029 (2004) [Erratum-ibid. D **71**, 099901 (2005)] [arXiv:nucl-th/0405079]; A. Gerhold and A. Rebhan, Phys. Rev. D **71**, 085010 (2005) [arXiv:hep-ph/0501089]; P. T. Reuter, arXiv:nucl-th/0602043; J. L. Noronha, H. c. Ren, I. Giannakis, D. Hou and D. H. Rischke, Phys. Rev. D **73**, 094009 (2006) [arXiv:hep-ph/0602218]; D. Nickel, J. Wambach and R. Alkofer, Phys. Rev. D **73**, 114028 (2006) [arXiv:hep-ph/0603163]; B. Feng, D. f. Hou, J. r. Li and H. c. Ren, Nucl. Phys. B **754**, 351 (2006) [arXiv:nucl-th/0606015]; P. T. Reuter, Phys. Rev. D **74**, 105008 (2006) [arXiv:nucl-th/0608020].
 - [13] M. Buballa, Phys. Rept. **407**, 205 (2005) [arXiv:hep-ph/0402234]; S. B. Rüster, V. Werth, M. Buballa, I. A. Shovkovy and D. H. Rischke, Phys. Rev. D **72**, 034004 (2005) [arXiv:hep-ph/0503184].
 - [14] K. Nawa, E. Nakano and H. Yabu, Phys. Rev. D **74**, 034017 (2006) [arXiv:hep-ph/0509029]; A. H. Rezaeian and H. J. Pirner, Nucl. Phys. A **779**, 197 (2006) [arXiv:nucl-th/0606043].
 - [15] M. Kitazawa, D. H. Rischke and I. A. Shovkovy, Phys. Lett. B **637**, 367 (2006) [arXiv:hep-ph/0602065].
 - [16] Y. Nishida and H. Abuki, Phys. Rev. D **72**, 096004 (2005) [arXiv:hep-ph/0504083].
 - [17] H. Abuki, arXiv:hep-ph/0605081.
 - [18] L. He and P. Zhuang, arXiv:hep-ph/0703042.
 - [19] R. Friedberg and T. D. Lee, Phys. Rev. B **40**, 6745 (1989); R. Friedberg, T. D. Lee and H. C. Ren, Phys. Rev. B **42**, 4122 (1990).
 - [20] M. Holland, S.J.J.M.F. Kokkelmans, M.L. Chiofalo, R. Walser, Phys. Rev. Lett. **87**, 120406 (2001) [arXiv:cond-mat/0103479]; M.L. Chiofalo, S.J.J.M.F. Kokkelmans, J.N. Milstein, M.J. Holland, Phys. Rev. Lett. **88**, 090402 (2001) [arXiv:cond-mat/0110119]; E. Timmermans, K. Furuya, P.W. Milonni, A.K. Kerman, Phys. Lett. A **285**, 228 (2001) [arXiv:cond-mat/0103327]; Y. Ohashi and A. Griffin, Phys. Rev. Lett. **89**, 130402 (2002).
 - [21] J. Ranninger in *Bose-Einstein condensation*, edited by A. Griffin, D.W. Snoke, and S. Stringari (Cambridge University Press, Cambridge, 1995); T. Domanski, J. Ranninger, Physica C **387**, 77 (2003) [arXiv:cond-mat/0208255].
 - [22] K. Rajagopal and A. Schmitt, Phys. Rev. D **73**, 045003 (2006) [arXiv:hep-ph/0512043].
 - [23] J.I. Kapusta, *Finite-temperature field theory* (Cambridge University Press, Cambridge, 1989).
 - [24] S.Y. Chang, J. Carlson, V.R. Pandharipande, K.E. Schmidt, Phys. Rev. A **70**, 043602 (2004) [arXiv:physics/0404115].

- [25] J. Carlson and S. Reddy, Phys. Rev. Lett. **95**, 060401 (2005) [arXiv:cond-mat/0503256].
- [26] Y. Nishida and D. T. Son, Phys. Rev. Lett. **97**, 050403 (2006) [arXiv:cond-mat/0604500]; A. Bulgac and M. M. Forbes, arXiv:cond-mat/0606043; G. Rupak, T. Schäfer and A. Kryjevski, arXiv:cond-mat/0607834; Y. Nishida and D. T. Son, arXiv:cond-mat/0607835; J.-W. Chen, E. Nakano, arXiv:cond-mat/0610011.
- [27] M. Alford and Q. h. Wang, J. Phys. G **31**, 719 (2005) [arXiv:hep-ph/0501078].
- [28] Q. Chen, J. Stajic, S. Tan, K. Levin, Phys. Rep. **412**, 1 (2005); K. Levin, Q. Chen, arXiv:cond-mat/0610006.
- [29] M. Kitazawa, T. Koide, T. Kunihiro and Y. Nemoto, Prog. Theor. Phys. **114**, 117 (2005) [arXiv:hep-ph/0502035]; M. Kitazawa, T. Kunihiro and Y. Nemoto, Phys. Lett. B **631**, 157 (2005) [arXiv:hep-ph/0505070].
- [30] J. Deng, A. Schmitt and Q. Wang, in preparation.
- [31] E. Gubankova, W. V. Liu and F. Wilczek, Phys. Rev. Lett. **91**, 032001 (2003) [arXiv:hep-ph/0304016].
- [32] M. Huang and I. A. Shovkovy, Phys. Rev. D **70**, 051501 (2004) [arXiv:hep-ph/0407049]; R. Casalbuoni, R. Gatto, M. Mannarelli, G. Nardulli and M. Ruggieri, Phys. Lett. B **605**, 362 (2005) [Erratum-ibid. B **615**, 297 (2005)] [arXiv:hep-ph/0410401].
- [33] A. I. Larkin and Yu. N. Ovchinnikov, Zh. Eksp. Teor. Fiz. **47**, 1136 (1964)[Sov. Phys. JETP **20**, 762 (1965)]; P. Fulde and R. A. Ferrell, Phys. Rev. **135**, A550 (1964).